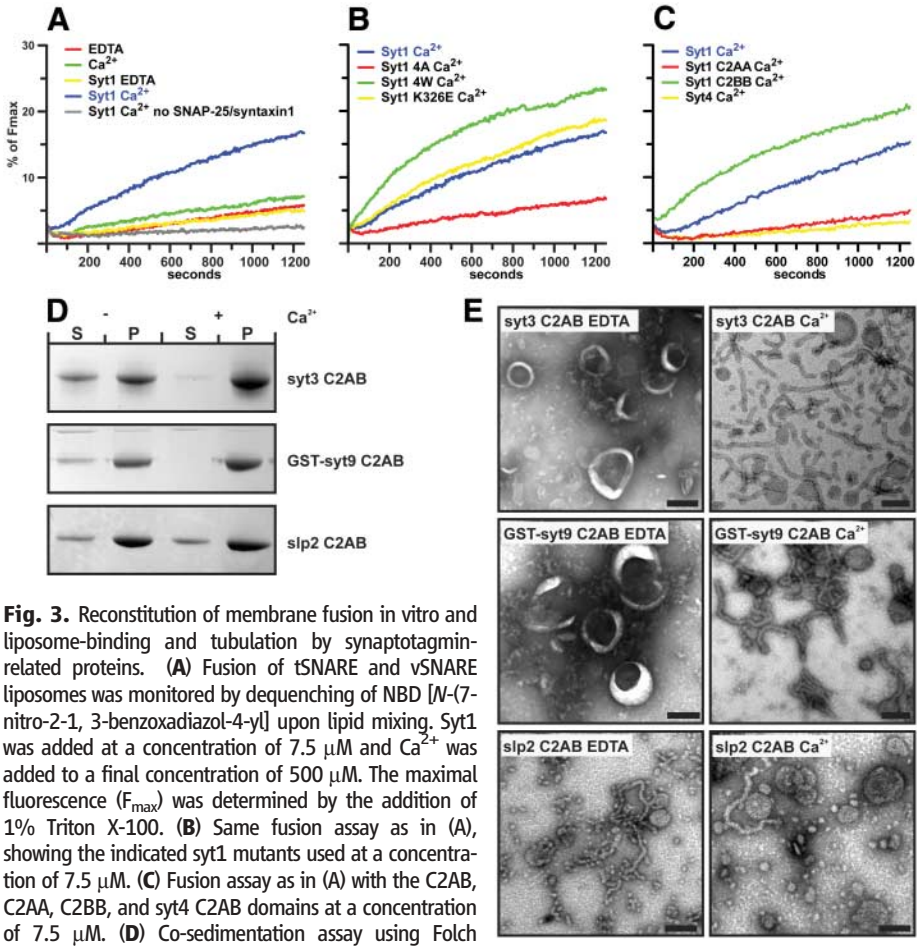

Fig. 3. Reconstitution of membrane fusion in vitro and liposome-binding and tubulation by synaptotagmin-related proteins. (**A**) Fusion of tSNARE and vSNARE liposomes was monitored by dequenching of NBD [*N*-(7-nitro-2-1, 3-benzoxadiazol-4-yl] upon lipid mixing. Syt1 was added at a concentration of 7.5 μM and Ca^{2+} was added to a final concentration of 500 μM. The maximal fluorescence (F_{max}) was determined by the addition of 1% Triton X-100. (**B**) Same fusion assay as in (A), showing the indicated syt1 mutants used at a concentration of 7.5 μM. (**C**) Fusion assay as in (A) with the C2AB, C2AA, C2BB, and syt4 C2AB domains at a concentration of 7.5 μM. (**D**) Co-sedimentation assay using Folch liposomes and the indicated proteins. (**E**) Electron micrographs of Folch liposomes incubated with the indicated proteins. Ca^{2+} was added to a final concentration of 1 mM in (D) and (E). Scale bar: 100 nm.

3. I. Fernandez *et al.*, *Neuron* **32**, 1057 (2001).
4. B. A. Davletov, T. C. Sudhof, *J. Biol. Chem.* **268**, 26386 (1993).
5. R. Fernandez-Chacon *et al.*, *Nature* **410**, 41 (2001).
6. J. S. Rhee *et al.*, *Proc. Natl. Acad. Sci. U.S.A.* **102**, 18664 (2005).
7. J. Tang *et al.*, *Cell* **126**, 1175 (2006).
8. L. V. Chernomordik, M. M. Kozlov, *Annu. Rev. Biochem.* **72**, 175 (2003).
9. Y. Kozlovsky, M. M. Kozlov, *Biophys. J.* **82**, 882 (2002).
10. R. B. Sutton, B. A. Davletov, A. M. Berghuis, T. C. Sudhof, S. R. Sprang, *Cell* **80**, 929 (1995).
11. Materials and methods and calculations are available as supporting material on *Science* Online.
12. M. S. Perin, V. A. Fried, G. A. Mignery, R. Jahn, T. C. Sudhof, *Nature* **345**, 260 (1990).
13. J. Bai, W. C. Tucker, E. R. Chapman, *Nat. Struct. Mol. Biol.* **11**, 36 (2004).
14. E. Hui, J. Bai, E. R. Chapman, *Biophys. J.* **91**, 1767 (2006).
15. D. Z. Herrick, S. Sterbling, K. A. Rasch, A. Hinderliter, D. S. Cafiso, *Biochemistry* **45**, 9668 (2006).
16. Single-letter abbreviations for the amino acid residues used are as follows: A, Ala; D, Asp; F, Phe; K, Lys; L, Leu; M, Met; V, Val; and W, Trp.
17. B. J. Peter *et al.*, *Science* **303**, 495 (2004).
18. I. M. Robinson, R. Ranjan, T. L. Schwarz, *Nature* **418**, 336 (2002).
19. J. M. Mackler, J. A. Drummond, C. A. Loewen, I. M. Robinson, N. E. Reist, *Nature* **418**, 340 (2002).
20. T. Weber *et al.*, *Cell* **92**, 759 (1998).
21. W. C. Tucker, T. Weber, E. R. Chapman, *Science* **304**, 435 (2004).
22. H. Dai, N. Shen, D. Arac, J. Rizo, *J. Mol. Biol.* **367**, 848 (2007).
23. C. Rickman, M. Craxton, S. Osborne, B. Davletov, *Biochem. J.* **378**, 681 (2004).
24. C. Rickman *et al.*, *Mol. Biol. Cell* **17**, 283 (2006).
25. P. I. Kuzmin, J. Zimmerberg, Y. A. Chizmadzhev, F. S. Cohen, *Proc. Natl. Acad. Sci. U.S.A.* **98**, 7235 (2001).
26. A. Bhalla, M. C. Chicka, W. C. Tucker, E. R. Chapman, *Nat. Struct. Mol. Biol.* **13**, 323 (2006).
27. X. Shao, I. Fernandez, T. C. Sudhof, J. Rizo, *Biochemistry* **37**, 16106 (1998).
28. Y. Cheng *et al.*, *Protein Sci.* **13**, 2665 (2004).

29. We thank B. Davletov for the provision of synaptotagmin 3, 4, and 9 plasmids and members of the lab for extensive discussions. This work was supported by the Medical Research Council (UK). We also gratefully acknowledge a long-term fellowship from the European Molecular Biology Organization (ALTF 21-2006) to S.M. and the Israel Science Foundation, United States–Israel Binational Science Foundation, and the Marie Curie Network "Flippases" funding for M.M.K.

Supporting Online Material

www.sciencemag.org/cgi/content/full/316/5828/1205/DC1
Materials and Methods
SOM Text
Figs. S1 to S6
References

12 January 2007; accepted 17 April 2007
Published online 3 May 2007;
10.1126/science.1142614
Include this information when citing this paper.

Myosin V Walks by Lever Action and Brownian Motion

Katsuyuki Shiroguchi and Kazuhiko Kinosita Jr.*

Myosin V is a molecular motor that moves cargo along actin filaments. Its two heads, each attached to a long and relatively stiff neck, move alternately forward in a "hand-over-hand" fashion. To observe under a microscope how the necks move, we attached a micrometer-sized rod to one of the necks. The leading neck swings unidirectionally forward, whereas the trailing neck, once lifted, undergoes extensive Brownian rotation in all directions before landing on a site ahead of the leading head. The neck-neck joint is essentially free, and the neck motion supports a mechanism where the active swing of the leading neck biases the random motion of the lifted head to let it eventually land on a forward site.

Linear molecular motors such as myosin, kinesin, or dynein are often Y-shaped, with two identical arms of Y each ending in a globular motor domain that binds to a track in an adenosine triphosphate (ATP)–dependent manner. Traditionally the motor domain has been called a "head" and the rest of the arm a "neck" (Fig. 1A). How the heads and necks cooperate to propel the motor is best understood in those motors that take many discrete steps without falling off a filamentous track (*1*–*7*): The two heads move forward alternately in a "hand-over-hand" fashion, as in human walking (*8*–*11*). However, the mechanism for bringing the lagging head onto a forward landing site is not yet firmly established. Here we focus on myosin V (*12*, *13*) that walks on an actin filament with ~35-nm steps (*14*, *15*). The necks of this motor are stiff relative to those of other motors such as kinesin, and they are called "lever arms" because they would serve as a lever. In electron micrographs (*16*), myosin V's long necks form a V-shape when both heads are attached to actin. Every step would thus result in leaning of a neck alternately forward and backward, as indeed was shown when a fluorophore

Department of Physics, Faculty of Science and Engineering, Waseda University, Okubo 3-4-1, Shinjuku-ku, Tokyo 169-8555, Japan.

*To whom correspondence should be addressed. E-mail: kazuhiko@waseda.jp

was attached to a neck (*17*, *18*). Our aim here was to resolve the neck motion during the transition between the two static orientations, and to infer the force behind the motion. Translational motion of a neck during the transients was recently reported (*19*). To examine rotational motion, we attached a micrometer-sized, fluorescently labeled microtubule to one of the necks of myosin V.

We replaced calmodulin light chains that wrap around the necks (Fig. 1A) with an engineered fusion protein in which calmodulin was connected to a motor domain of a mutated kinesin (*20*) that irreversibly binds to a microtubule (Fig. 1B). Then we added fluorescently labeled microtubules, hoping that in some myosin molecules only one of the two necks would bind a microtubule at multiple points. An actin filament was suspended in solution by holding two polystyrene beads attached to the filament ends with dual optical tweezers (*21*). By moving the microscope stage, we manipulated a floating microtubule, typically 2 to 3 μm long and binding at most eight myosin V molecules per μm, onto the actin filament. On rare occasions, the microtubule bound to actin, presumably through myosin V, and swung to and fro several times, primarily in the image plane (Fig. 1; see also fig. S1 and movies S1 and S2). We think the swings reflect the myosin neck motion because (i) the two relatively stationary angles (blue and red horizontal bars in Fig. 1D and fig. S1) were separated by ~100° (±20° SD for 17 swings), consistent with the angles between the V-shaped necks in the electron micrographs (*16*); (ii) dwell times on the stationary angles averaged 3 to 4 s, as expected for ATP-initiated swings at 0.2 to 0.3 μM ATP with a rate of ATP binding (*22*) of 0.9×10^6 M^{-1} s^{-1}; and (iii) the swings accompanied microtubule translocation. Swings in one direction (from blue to red bars) were always unidirectional, indicative of a power stroke. The other direction often involved extensive fluctuations, as in Fig. 1D at 15 to 17 s, suggesting Brownian search of a lifted neck for a next binding site. The micrometer-sized microtubule probe thus allowed us to visualize neck motion and confirm the expected behavior, but we were unable to obtain sufficient data to study details of the stepping dynamics.

We thus tried a reverse scheme (Fig. 2A): Instead of fixing an actin filament in space, we fixed a microtubule carrying myosin V (0.3 to 1 molecule μm^{-1}) on a glass surface and waited for a short (~1 μm) actin filament to land on it and move. For myosin V on the top surface of a microtubule 25 nm in diameter, movement of the actin filament in a horizontal plane would not be hindered by the glass surface. Note that the bound neck of myosin V is not necessarily parallel to the thick microtubule consisting of 13 tubulin protofilaments (Fig. 2A). In this reverse configuration, the actin filament would swing between two stationary angles where both heads of myosin V bind the filament. In between, the filament would be carried by one neck and would report the orientation of the actin-binding surface of the head. The actin filament would be translocated, with respect to the neck immobilized on the microtubule, by ~70 nm in the swing 3 → 5 in Fig. 2A; no translocation would accompany the swing 1 → 3. If a free joint(s) existed between two necks, the actin filament would undergo rotational Brownian fluctuation during swings accompanying the ~70-nm translocation, whereas the opposite swings would be unidirectional.

We observed the expected motions, and we analyzed 11 actin filaments that met the criteria of four or more swings between two stationary angles and translocation per swing of >25 nm (Figs. 2 and 3, fig. S5, and movies S3 and S4). A prominent feature was the asymmetry of swings (Fig. 2C and fig. S5), clearly noticeable because of the fast motions of short actin relative to longer microtubules above. Actin swings in one direction (39 swings, shown as anticlockwise and positive-going angular transitions in all figures) were accompanied by little translocation (–9 ± 23 nm, Fig. 3A), ended within ~50 ms (fig. S2), and were always unidirectional (Fig. 3B). Opposite, clockwise swings (38 swings) were accompanied by a large translocation averaging 73 ± 28 nm (Fig. 3A) except for three irregularities possibly due to backstepping (green arrow in Fig. 2C). Most of the clockwise swings involved fluctuations in either direction (Fig. 3C), continuing for

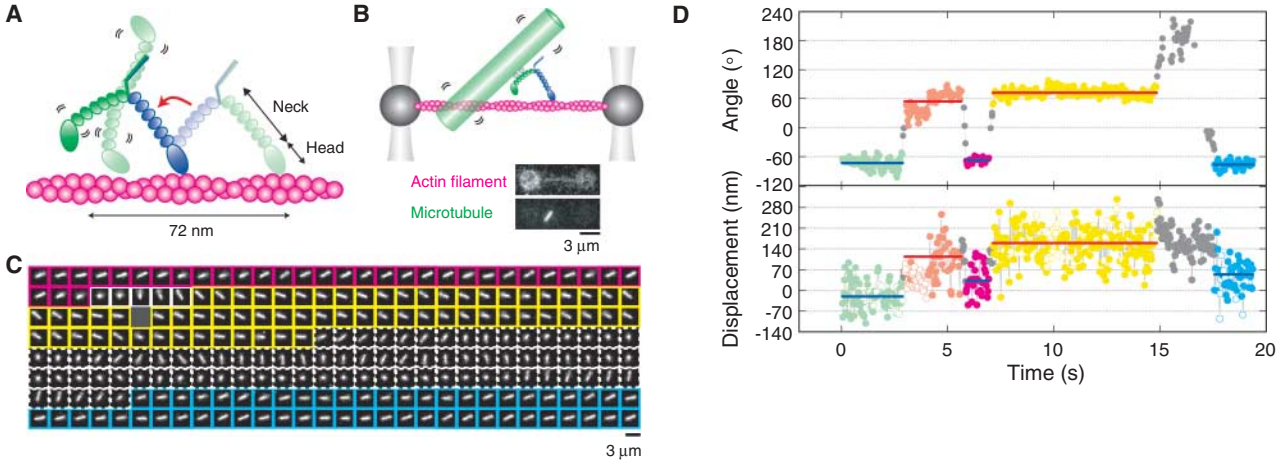

Fig. 1. Observation of neck motion in myosin V. (**A**) Postulated walking scheme for myosin V. Myosin V has two long necks (blue and green) reinforced with six calmodulin light chains (small ellipsoids) and catalytic heads (large ellipsoids) that hydrolyze ATP. Walking (toward left) on an actin filament (magenta) begins with binding of ATP to the trailing head to dissociate it from actin. The leading neck (blue) then leans forward (lever action: red arrow), powered by ATP hydrolysis (presumably phosphate release) in the leading head. The lifted neck (green) fluctuates around the neck-neck junction until the head binds to a site ~35 nm ahead of the blue head. (**B**) Observation of neck motion through a microtubule (light green cylinder) attached to a neck by linking calmodulins to a mutated kinesin (small gray circles) that irreversibly binds to a microtubule. Necks of myosin and thicknesses of the actin filament and microtubule are approximately to scale. The actin filament was bound to beads coated with α-actinin (dark gray) and held by dual-beam optical tweezers. The images of actin (and beads) stained with Alexa 488 and of a microtubule stained with tetramethylrhodamine were captured simultaneously. (**C**) Sequential images at 33-ms intervals of a microtubule, carrying fewer than four myosin V molecules per μm, apparently walking toward the left at 0.2 μM ATP. Magenta, yellow, and blue frames show two relatively stable angles; white solid frames, a unidirectional swing; white dotted frames, fluctuations; dark gray image, omission of 166 frames. Part of movie S1. (**D**) Upper panel: Swing angle anticlockwise from 0 o'clock; stationary angles are colored as in (C), and bars show the average. Swings are shown in gray. Omissions indicate orientations nearly vertical to the image plane. Lower panel: Movement of the centroid of the microtubule image calculated within a horizontal band of height 600 nm along the actin filament. Bars indicate averages over solid dots where the microtubule remained within 15° from the average stationary angle (open dots, orientations beyond 15°). Only comparisons among blue bars, or among red bars, are meaningful, because the centroids depended on the microtubule orientation to some extent.

0.6 s on average. The fluctuation period was distributed roughly exponentially, accounting for the apparent absence of fluctuations in some swings (fig. S3). Net translocation per swing pair was 62 ± 21 nm (Fig. 3D), somewhat smaller than the 70 nm obtained in experiments where beaded myosin V was allowed to spiral around actin (*15*). Here, actin displacement estimated from the centroid of the whole actin image is intrinsically imprecise, and the actin filament may have rotated around its axis to allow shorter steps. Dwells on the two stationary angles both averaged 7 to 8 s (fig. S4), consistent with the expected (*22*) ATP-waiting dwell of 5.6 s at 0.2 μM ATP. In the stationary phases, we sometimes noticed small angular steps (e.g., at ~52 s and several other places in Fig. 2C) that might indicate the existence of two V-shaped postures in the two-head bound state, such as bending of a neck(s) or shift of a head onto a neighboring actin monomer. Such substeps were not always observed and the direction was variable (fig. S5); thus, steric hindrance (e.g., between actin and microtubule surfaces) can also account for this phenomenon.

In the fluctuation phase, the mean square angle increased linearly with time (Fig. 3E). The slope gives a rotational diffusion constant of 11 $rad^2\ s^{-1}$. This value is close to 17 $rad^2\ s^{-1}$ calculated for a rod of diameter 10 nm and length 0.6 μm (average actin length between the myosin attachment and farther end) rotating around one end in water. The fluctuation angle eventually spreads over >600° (Fig. 3C). Thus, the fluctuation represents basically unhindered rotational diffusion in water, although actin occasionally gets stuck for a while. The free diffusion is consistent with the presence of a free joint at the neck-neck junction, as indicated earlier for myosin II (*23*) and myosin V (*16*). Two-headed motors with necks in basic twofold symmetry cannot walk without flexible joints (*24*, *25*). Our study further indicates that the joint is almost completely free, in that thermal agitation suffices to let an unattached neck assume all orientations in space (see below for three-dimensional fluctuations). Dunn and Spudich (*19*) attached a 40-nm gold particle to a neck of walking myosin V and showed that the particle undergoes rapid translational diffusion between two stationary phases where, presumably, both heads are bound to actin. Our results are consistent with their finding and further indicate that the diffusion is primarily of rotational nature.

Anticlockwise swings, in contrast, were always unidirectional, without a significant sign of reversal (at the video resolution of 33 ms), indicating that they are driven by active force. These swings without translocation are made by reorientation of the head on the neck immobilized on a microtubule (Fig. 2A). Our observation clearly shows that this reorientation, if viewed on actin, results in leaning of the neck forward (lever action), toward the direction in which myosin V would move, because actin is translocated by ~70 nm rearward at the completion of the next, fluctuating clockwise swing. The final phase of the anticlockwise swing may be assisted by binding of the free head, leading to the next

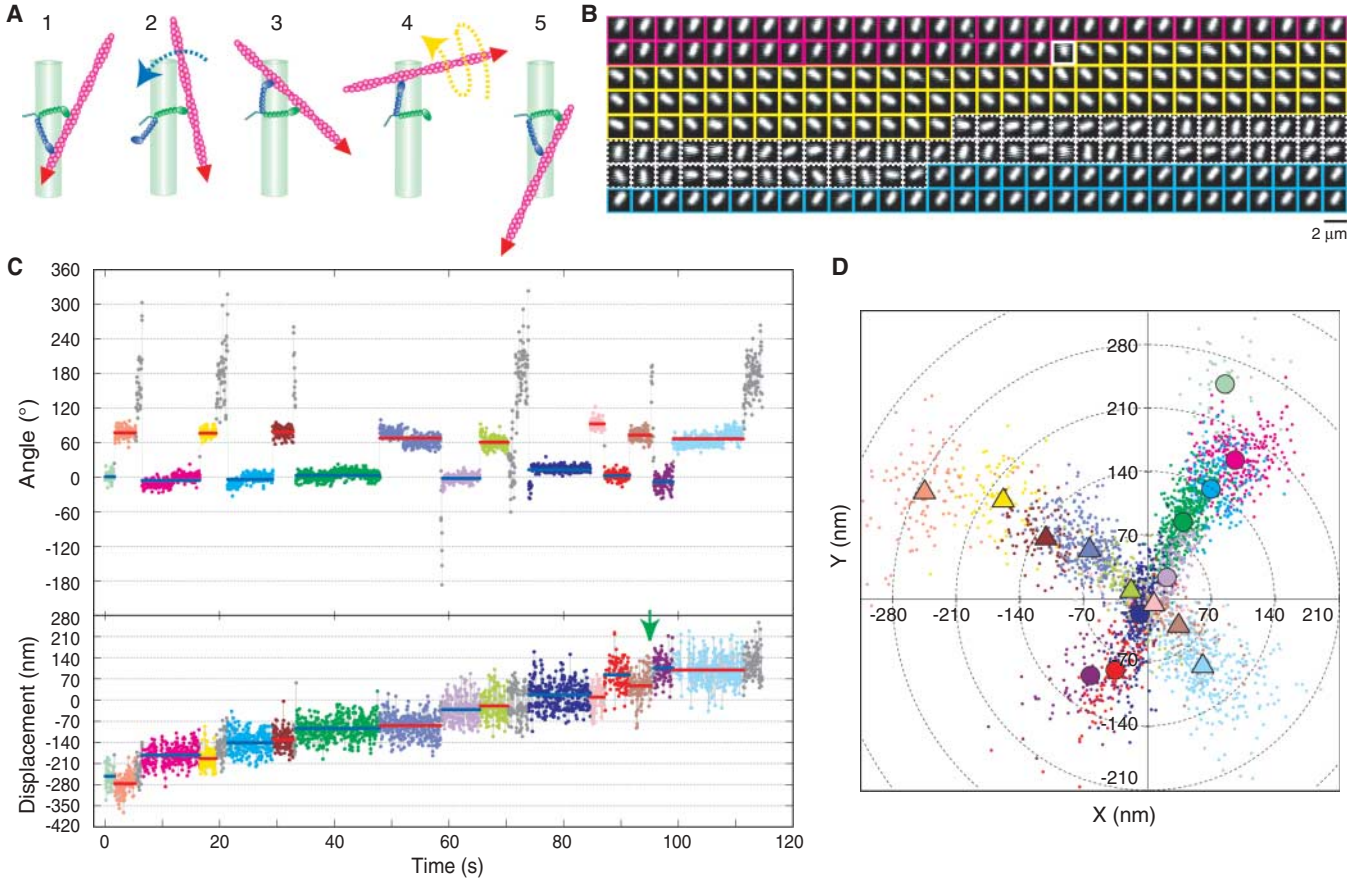

Fig. 2. Actin motion in the actin moving assay on a surface. (**A**) Expected movement of an actin filament (magenta) driven by myosin V with one neck (green) attached to a microtubule (light green cylinder) lying on a glass surface. One swing (blue arrow), mainly by lever action, is quick and unidirectional, whereas the other swing (yellow arrow) goes through Brownian fluctuation before final attachment. At the completion of the return swing, the actin filament proceeds by ~70 nm. Red arrowheads indicate the pointed end toward which the actin filament moves. The thick microtubule and myosin neck (approximately to scale) are not necessarily parallel, and the configuration here applies to (B) to (D) below. (**B**) Sequential images at 33-ms intervals of a moving actin filament at 0.2 μM ATP. Colors are as in (C). Part of movie S3. (**C**) Time courses of angular [anticlockwise from 1 in (A), unrestricted in the fluctuation phase] and positional changes. Displacements were estimated from (D). Blue and red bars, average of the stationary angles; green arrow, possible backstepping. (**D**) Frame-by-frame plot of the centroid of the actin filament image while it was in two stationary angles. Circles and triangles denote averaged positions; colors are as in (C).

stationary angle. Veigel *et al*. (*26*) showed that a one-neck construct of myosin V forces actin to move for ~25 nm by hydrolyzing one ATP molecule and that the movement can oppose a backward force of a few piconewtons. They proposed that the movement represents ATP-powered lever action of the neck and that, during 36-nm step walking of two-headed myosin V, the difference between the step size of 36 nm and the lever action of ~25 nm would be covered by diffusion of the lifted head. Similar results have been reported by Moore *et al*. (*27*). Our observations confirm the rotational nature of the lever action and its expected direction, as well as the presence of a diffusive phase. Nucleotide-dependent conformational changes corresponding to a lever action have been seen in crystal structures (*28*), although so far only in the absence of actin.

The swing angle, the difference between the two stationary angles, averaged 92° ± 21° (Fig. 3F), whereas single-fluorophore assays (*17*, *18*) have reported 70° to 75°. Presumably, the swing angle equals the angle between necks when myosin V stands on actin with both heads attached. In electron micrographs (*16*), the leading neck was often curved forward as in the telemark stance. Our swing angle is close to the average angle between whole necks. Fluorophores probably bound to a lower part of a neck.

To find the 11 actin filaments that satisfied the criteria for analysis, we observed >1000 filaments that apparently bound to a microtubule, but most did not move. The low success rate was anticipated, because binding of only one of the two necks to a microtubule through multiple points, in an orientation that does not hinder actin binding and subsequent lever action, must be a rare circumstance; furthermore, bound actin must be precisely parallel to the glass surface to swing freely. Also, because myosin density on a microtubule could not be too low, actin swing often ceased when the actin filament became parallel to the microtubule, presumably by binding to a second myosin.

One could argue that the asymmetric behavior described above may have resulted from surface obstructions. We therefore performed the

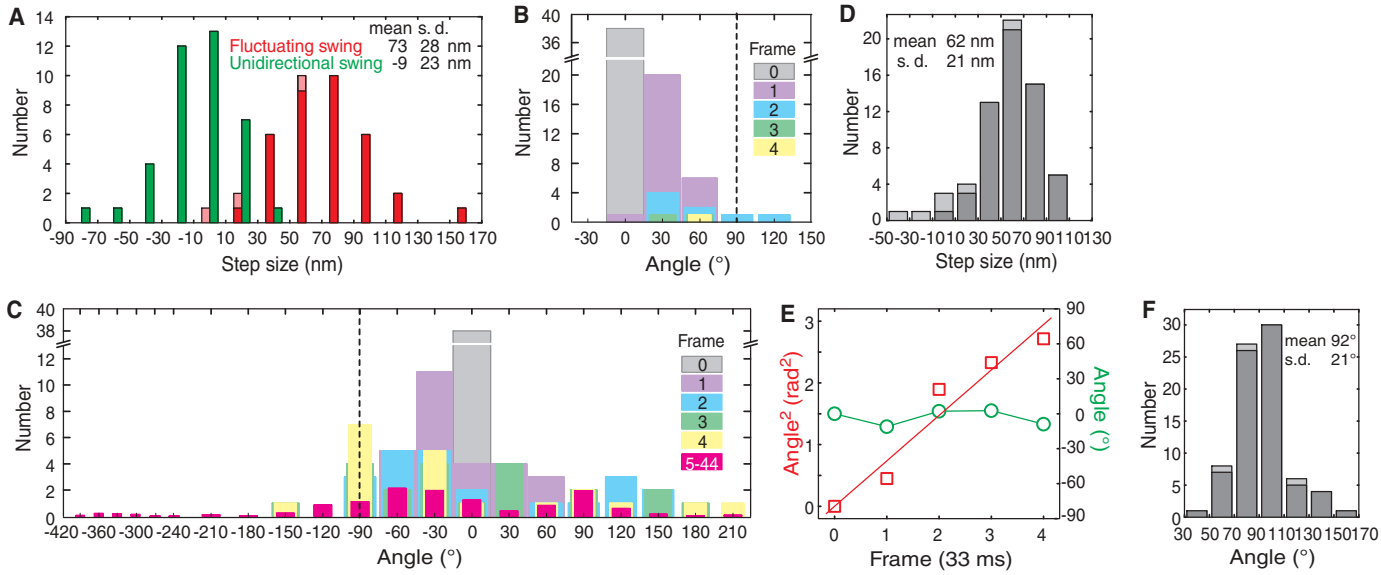

Fig. 3. Analyses of the swings in the actin moving assay on a surface. (**A**) Translocation during an anticlockwise (green) or clockwise (red) swing: displacement from blue to red bars and from red to blue, respectively, in Fig. 2C and fig. S5. Apparent backsteps (light colors) are excluded from the mean. (**B** and **C**) Angle histograms at indicated frames (33 ms per frame) during anticlockwise unidirectional (B) and clockwise fluctuating (C) swings of 11 actin filaments in Fig. 2C and fig. S5. Time and angle immediately before a swing are taken as frame 0 and 0°. Swings terminate, on average, at the dashed line showing the next stationary angle. Magenta in (C), average over frames 5 to 44. (**D**) Steps per swing pair: blue to blue and red to red in Fig. 2C and fig. S5. Apparent backsteps (light gray) are excluded from mean. (**E**) Average angular evolution in the clockwise, fluctuating swings. Slope of the red line, twice the rotational diffusion constant, is 22 rad^2 s^{-1}. (**F**) Amplitudes of all 77 swings. Light gray, apparent backstep.

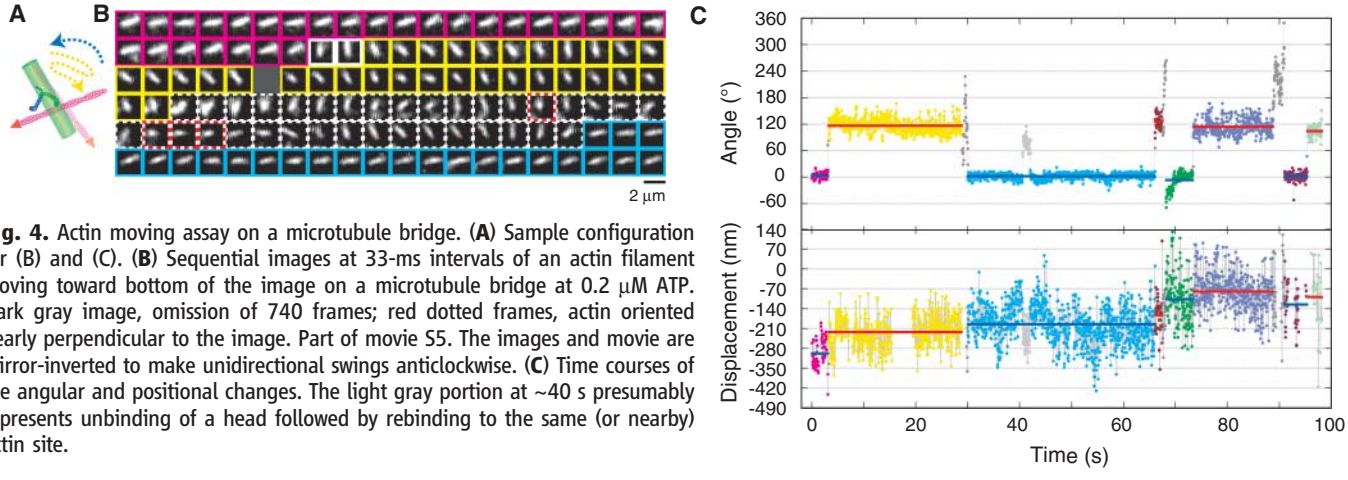

Fig. 4. Actin moving assay on a microtubule bridge. (**A**) Sample configuration for (B) and (C). (**B**) Sequential images at 33-ms intervals of an actin filament moving toward bottom of the image on a microtubule bridge at 0.2 μM ATP. Dark gray image, omission of 740 frames; red dotted frames, actin oriented nearly perpendicular to the image. Part of movie S5. The images and movie are mirror-inverted to make unidirectional swings anticlockwise. (**C**) Time courses of the angular and positional changes. The light gray portion at ~40 s presumably represents unbinding of a head followed by rebinding to the same (or nearby) actin site.

actin moving assay on a microtubule bridge (*21*), a modification of the actin-bridge assay (*15*), by suspending a microtubule between two large beads immobilized on a glass surface to let the actin filament freely rotate in any direction. We found three swinging actin filaments that stayed primarily in the image plane and that were simultaneously translocated. All showed asymmetric swings (Fig. 4, fig. S6, and movies S5 and S6). When these filaments fluctuated, we saw moments when the filament became perpendicular to the image plane, appearing as a bright dot (red dotted frames in Fig. 4B; also Fig. 1C). Apparently the free neck could assume all orientations in space.

By attaching a micrometer-sized rod to a neck of the nanometer-sized molecular motor, we have been able to infer the neck motion continuously in real time. Viscous friction on the rod must slow down the motion, but essential features are likely preserved, as shown for the rotation of F_1-ATPase (*29*). The two necks of myosin V are connected via a free joint. Thus, the sole mechanism that can move a lifted head is Brownian rotation of the neck, but this is purely random, carrying the head in either direction with an equal probability. Ensuring forward landing thus requires a biasing mechanism(s). ATP-powered lever action of the landed neck, originally proposed for myosin II (*30*), moves forward the pivot of the Brownian rotation, producing the required bias, as has been suggested in electron microscopy and single-molecule studies (*16*, *19*, *26*, *27*). The rotational diffusion observed here implies that the lifted head stays off the actin surface for most of the time, as opposed to diffusional sliding of the myosin head along the actin surface (*31*). The rotational diffusion plus lever action, however, may not be sufficient. We have proposed that, to ensure forward landing of a lifted head in the presence of backward load, the track-binding surface of the head must be properly oriented such that forward swing of the neck makes the surface parallel with the track surface (*24*, *25*, *32*). One way to prove this orientational biasing experimentally is to attach a micrometer-sized rod. A rod that directly reports molecular orientations will be useful in studies where a conformational change in a protein machine, necessarily accompanying reorientation, is to be visualized during function.

References and Notes

1. K. Svoboda, C. F. Schmidt, B. J. Schnapp, S. M. Block, *Nature* **365**, 721 (1993).
2. R. D. Vale, *J. Cell Biol.* **163**, 445 (2003).
3. J. R. Sellers, C. Veigel, *Curr. Opin. Cell Biol.* **18**, 68 (2006).
4. R. S. Rock *et al.*, *Proc. Natl. Acad. Sci. U.S.A.* **98**, 13655 (2001).
5. S. Nishikawa *et al.*, *Biochem. Biophys. Res. Commun.* **290**, 311 (2002).
6. R. Mallik, B. C. Carter, S. A. Lex, S. J. King, S. P. Gross, *Nature* **427**, 649 (2004).
7. S. Toba, T. M. Watanabe, L. Yamaguchi-Okimoto, Y. Y. Toyoshima, H. Higuchi, *Proc. Natl. Acad. Sci. U.S.A.* **103**, 5741 (2006).
8. A. Yildiz *et al.*, *Science* **300**, 2061 (2003); published online 5 June 2003 (10.1126/science.1084398).
9. A. Yildiz *et al.*, *J. Biol. Chem.* **279**, 37223 (2004).
10. A. Yildiz, M. Tomishige, R. D. Vale, P. R. Selvin, *Science* **303**, 676 (2004); published online 18 December 2003 (10.1126/science.1093753).
11. S. L. Reck-Peterson *et al.*, *Cell* **126**, 335 (2006).
12. E. M. Espreafico *et al.*, *J. Cell Biol.* **119**, 1541 (1992).
13. R. E. Cheney *et al.*, *Cell* **75**, 13 (1993).
14. A. D. Mehta *et al.*, *Nature* **400**, 590 (1999).
15. M. Y. Ali *et al.*, *Nat. Struct. Biol.* **9**, 464 (2002).
16. M. L. Walker *et al.*, *Nature* **405**, 804 (2000).
17. J. N. Forkey, M. E. Quinlan, M. A. Shaw, J. E. Corrie, Y. E. Goldman, *Nature* **422**, 399 (2003).
18. E. Toprak *et al.*, *Proc. Natl. Acad. Sci. U.S.A.* **103**, 6495 (2006).
19. A. R. Dunn, J. A. Spudich, *Nat. Struct. Mol. Biol.* **14**, 246 (2007).
20. I. M. Crevel *et al.*, *EMBO J.* **23**, 23 (2004).
21. See supporting material on *Science* Online.
22. E. M. De La Cruz, A. L. Wells, S. S. Rosenfeld, E. M. Ostap H. L. Sweeney, *Proc. Natl. Acad. Sci. U.S.A.* **96**, 13726 (1999).
23. K. Kinosita Jr., S. Ishiwata, H. Yoshimura, H. Asai, A. Ikegami, *Biochemistry* **23**, 5963 (1984).
24. K. Kinosita Jr., K. Shiroguchi, M. Y. Ali, K. Adachi, H. Itoh, *Adv. Exp. Med. Biol.* **592**, 369 (2007).
25. K. Kinosita Jr., M. Y. Ali, K. Adachi, K. Shiroguchi, H. Itoh, *Adv. Exp. Med. Biol.* **565**, 205 (2005).
26. C. Veigel, F. Wang, M. L. Bartoo, J. R. Sellers, J. E. Molloy, *Nat. Cell Biol.* **4**, 59 (2002).
27. J. R. Moore, E. B. Krementsova, K. M. Trybus, D. M. Warshaw, *J. Cell Biol.* **155**, 625 (2001).
28. P.-D. Coureux, H. L. Sweeney, A. Houdusse, *EMBO J.* **23**, 4527 (2004).
29. R. Yasuda, H. Noji, M. Yoshida, K. Kinosita Jr., H. Itoh, *Nature* **410**, 898 (2001).
30. H. E. Huxley, *Science* **164**, 1356 (1969).
31. T. Okada *et al.*, *Biochem. Biophys. Res. Commun.* **354**, 379 (2007).
32. M. Y. Ali *et al.*, *Biophys. J.* **86**, 3804 (2004).

33. We thank M. Shio for designing a stable microscope stage, Y. Oguchi for help in myosin V purification, K. Adachi for an image analysis program, M. Fukatsu and K. Sakamaki for encouragement and lab management, and members of the Kinosita lab for discussions. Supported by Grants-in-Aid for Specially Promoted Research and the 21COE Program from the Ministry of Education, Sports, Culture, Science and Technology, Japan. K.S. was a Research Fellow of the Japan Society for the Promotion of Science.

Supporting Online Material

www.sciencemag.org/cgi/content/full/316/5828/1208/DC1
Materials and Methods
Figs. S1 to S6
Movies S1 to S6
References

26 January 2007; accepted 10 April 2007
10.1126/science.1140468

Hardwiring the Brain: Endocannabinoids Shape Neuronal Connectivity

Paul Berghuis,[1]* Ann M. Rajnicek,[2]* Yury M. Morozov,[3]* Ruth A. Ross,[2] Jan Mulder,[4] Gabriella M. Urbán,[5] Krisztina Monory,[6] Giovanni Marsicano,[6]† Michela Matteoli,[7] Alison Canty,[4] Andrew J. Irving,[8] István Katona,[5] Yuchio Yanagawa,[9] Pasko Rakic,[3] Beat Lutz,[6] Ken Mackie,[10]‡ Tibor Harkany[1]§

The roles of endocannabinoid signaling during central nervous system development are unknown. We report that CB_1 cannabinoid receptors (CB_1Rs) are enriched in the axonal growth cones of γ-aminobutyric acid–containing (GABAergic) interneurons in the rodent cortex during late gestation. Endocannabinoids trigger CB_1R internalization and elimination from filopodia and induce chemorepulsion and collapse of axonal growth cones of these GABAergic interneurons by activating RhoA. Similarly, endocannabinoids diminish the galvanotropism of *Xenopus laevis* spinal neurons. These findings, together with the impaired target selection of cortical GABAergic interneurons lacking CB_1Rs, identify endocannabinoids as axon guidance cues and demonstrate that endocannabinoid signaling regulates synaptogenesis and target selection in vivo.

In the cerebral cortex, information processing requires the precise temporal and spatial coordination of synaptic communication among excitatory pyramidal cells, inhibitory γ-aminobutyric acid–containing (GABAergic) interneurons, and subcortical afferents (*1*). Cortical neurons are born in progenitor zones that are distant from their final positions, and their layer-specific patterning is achieved through extensive migration in the developing cerebrum (*1*, *2*). En route to their destination, cortical neurons establish their synaptic connectivity patterns (*3*), thus providing the blueprint for their functional diversification.

In the adult central nervous system (CNS), presynaptic $G_{i/o}$ protein–coupled CB_1 cannabinoid receptors (CB_1Rs) (*4*) are the targets of marijuana (*Cannabis* spp.)–derived psychoactive phytocannabinoids and of the endocannabinoids anandamide (AEA) and 2-arachidonoylglycerol (2-AG). Endocannabinoids released from postsynaptic neurons serve as retrograde messengers that suppress neurotransmitter release at mature cortical synapses (*4*). During brain development, CB_1Rs are first expressed in early neural progenitors (*5*), with receptor levels increasing throughout neuronal specification and synaptogenesis (*6*). Although functionally active CB_1Rs are localized to developing axonal projections (*6*, *7*), it remains unknown whether endocannabinoids function as diffusible axon guidance factors before the growth cone differentiates into a presynaptic nerve terminal.

We defined the precise cellular distribution of CB_1Rs on neuronal precursors during cortical cell migration, axonal navigation, and synaptogenesis